Electrode Composite for Flexible Zinc–Manganese Dioxide Batteries through In Situ Polymerization of Polymer Hydrogel

Alla M. Zamarayeva, Akshaya Jegraj, Anju Toor, Veronika I. Pister, Cheryl Chang, Austin Chou, James W. Evans, and Ana Claudia Arias*

It remains important to maximize energy density of wearable batteries. In addition, such batteries should be compliant, safe, and environmentally sustainable. Intrinsically safe zinc–manganese dioxide (Zn/MnO_2) batteries are great candidates for powering wearables. However, achieving flexibility of these systems is hindered by the absence of a binder that ensures mechanical integrity of the MnO_2 electrode composite. Herein, a unique approach to fabricate a mechanically robust MnO_2 electrode is presented. Polyvinyl alcohol (PVA)/ polyacrylic acid (PAA) gel cross-linked in situ via thermal treatment is used as a binder for the electrode. Furthermore, energy density and rate capability of the printed battery electrodes are improved by replacing graphite with single-walled carbon nanotubes (CNTs). The batteries retain 93% capacity when the discharge rate is increased from C/10 to C/3, as well as 97% of their capacity after being flexed. In contrast, batteries based on conventional composition retain 60% and 23% of the capacity, respectively. Finally, the battery with the modified electrode has high areal energy density of 4.8 mWh cm^{-2} and volumetric energy density of 320 mWh cm^{-3}.

Fabricating electronics in a flexible wearable format has significant advantages for health monitoring and sensing.[1–5] High-fidelity sensor–skin interfaces improve signal-to-noise ratio through the intimate contact of the device and body.[1,6,7] In addition, ability to wear the devices directly on the skin can enable continuous monitoring of metabolites in bodily fluids like sweat.[8–11] Standalone operation of such electronic systems cannot be realized without power source, such as a battery.[12–15] If the battery is not equally compliant, it will negate the advantages of these flexible devices. Thus, flexible batteries play an important role in achieving the vision of wearable and conforming electronics.

Dr. A. Toor, V. I. Pister, Prof. A. C. Arias
Department of Electrical and Computer Engineering
University of California Berkeley
2626 Hearst Ave., Berkeley, CA 94720, USA
E-mail: acarias@berkeley.edu

A. M. Zamarayeva, A. Jegraj, C. Chang, A. Chou, Prof. J. W. Evans
Department of Materials Science and Engineering
University of California Berkeley
2607 Hearst Ave., Berkeley, CA 94720, USA

The ORCID identification number(s) for the author(s) of this article can be found under https://doi.org/10.1002/ente.201901165.

In addition to being compliant, such a battery has to meet the energy and power requirements of the wearable systems, to be safe and environmentally sustainable. Batteries based on zinc (Zn) are widely explored for powering wearable devices, due to high safety and environmental friendliness. Zn–air being one of the attractive options, due to its high theoretical energy density.[16,17] Innovations in materials' design were used to achieve good electrochemical and mechanical performance of these batteries. Up-to-date, growing catalyst nanomaterials onto the carbon cloths,[18–21] carbon fiber films,[22,23] nanowire arrays,[24] graphene materials,[25,26] and carbon nanotube (CNT) structures[27–29] have been demonstrated. These approaches enable freestanding flexible electrodes and also ensure high accessibility of catalytic sites and a low contact resistance.

Among mainstream battery chemistries with low-cost and well-established material production routs, zinc–manganese dioxide (Zn/MnO_2) is well suited for the purpose.[16] Due to its characteristics such as low material costs, high energy density, and exceptional safety, it has been widely commercialized in the rigid cylindrical format by Duracell®, for example. In a commercial system, Zn paste and MnO_2 paste are tightly packed in the can, which serves a dual function of casing and a current collector. Once removed from the rigid can, such paste-like electrodes disintegrate. Thus, achieving flexibility of Zn/MnO_2 system requires new engineering approaches.

To date, there have been few demonstrations of flexible Zn/MnO_2 batteries.[15,30–42] Several used commercially available materials with innovative components revolving around device design,[15,30–33,37–39] whereas other relied on the novel materials' synthesis, where materials are intrinsically flexible.[34–36] Zhi et al. demonstrated innovative approaches to fabricate rechargeable Zn/MnO_2 batteries for wearables.[40–42] Batteries comprised hydrogel electrolyte that enabled resilience to severe mechanical deformations and stresses,[42] as well as subzero temperatures.[40] In addition to rechargeable systems, there is a need to develop primary batteries to power disposable wearables, such as health monitoring patches. Blue Spark brand's temperature monitor for babies is one example of such

commercially available patch. Gaikwad et al. previously achieved high flexibility and energy density primary Zn/MnO_2 batteries through dip-coating battery slurry with commercially available components into the supporting membrane that served as a mechanical support for the resulting electrode.[15,30–33] Kaltenbruner et al. embedded electrode paste into an elastomeric matrix.[38] While the aforementioned approaches ensured flexibility, inactive components significantly reduced the amount of energy that can be stored per unit volume or per unit area of the battery. At the same time, it is important to maximize energy density because dimensions of the battery are often limited with the size of the device being powered. An optimum system would match the commercial product in terms of energy density and at the same time have a flexible form factor. In this work we use commercially available materials to achieve primary batteries with a volumetric energy density of $320\,mWh\,cm^{-3}$, which is in a range of a commercial AA alkaline battery.[43]
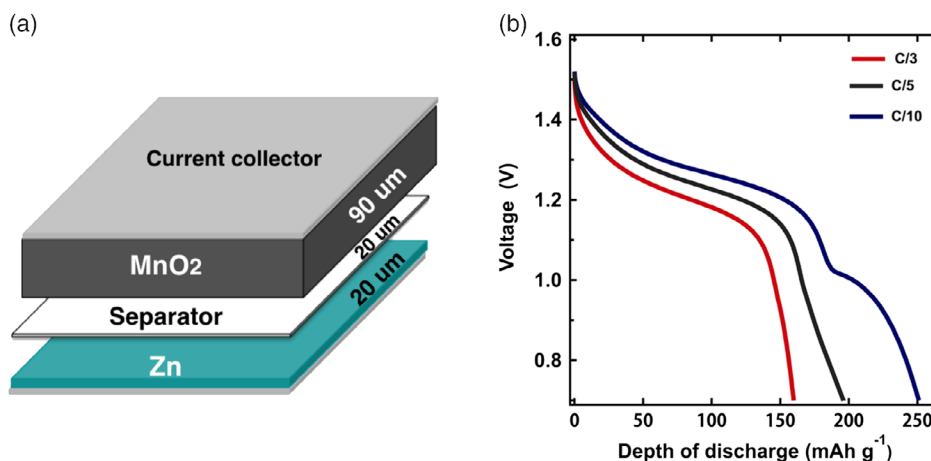
We fabricated compliant Zn/MnO_2 battery stack, where flexible Zn and MnO_2 electrodes were sandwiched with a commercially available separator. The electrodes were fabricated by casting electrode composites on the flexible substrate using doctor blade. As the capacity of the battery was limited by the mass of MnO_2 in the cathode, the thickness of MnO_2 electrode was increased to ≈4 times that of Zn electrode. Therefore, cracking and delamination of thicker MnO_2 cathode were limiting mechanical performance of the flexible batteries. One of the main challenges for realizing flexibility of MnO_2 electrode is the absence of a commercially available binder that would ensure mechanical integrity of the electrode composite. Binders available on the market are developed primarily for Li-ion battery chemistry. When utilized in the Zn/MnO_2 battery, such binders either disintegrate in alkaline media; or block the surface area of the active particles in a way that prevents electrolyte contact with the particle, and thus prohibits electrochemical reaction between active material and electrolyte; or simply do not provide sufficient adhesion. To realize printed, flexible Zn/MnO_2 batteries with high specific energy density, alternative solution had to be found to replace conventional binder.

An effective binder for the flexible electrode would accommodate mechanical deformation of the electrode and have strong adhesion to the electroactive particles and the conductive additive. The binder should also be chemically compatible with electrolyte and permeable to it. In this work we utilized polyvinyl alcohol (PVA) in situ cross-linked with polyacrylic acid (PAA) as a gel polymer binder for MnO_2 electrode. PVA/PAA membranes have been previously explored as solid polymer electrolytes for alkaline batteries.[44–46] The results from these studies indicate good stability of PVA/PAA in alkaline media and good conductivity (up to $10^{-2}\,S\,cm^{-1}$) of aqueous hydroxide species, which are the important electrode design considerations. In addition, mechanical properties of the PVA cross-linked with PAA have been previously studied for applications as a separation membrane material[47–54] and membranes for drug release.[53] The studies reveal that membranes obtained via cross-linking of PVA with 15–20% PAA exhibit high tensile strength ($900\,kg\,cm^{-2}$) without brittleness. These mechanical properties make cross-linked PVA/PAA a good candidate as a binder for flexible batteries. Song et al. used in situ thermal cross-linking

of PAA and PVA as a polymer binder for Si anodes in Li-ion batteries.[55] However, it has never been implemented in alkaline batteries. In this work, PVA/PAA gel was *mixed* with the rest of the electrode components and cross-linked in situ via thermal treatment. The binder formed 3D interpenetrated polymer network throughout the electrode, confining active material and conductive additive. Furthermore, to improve the energy density and rate capability of the printed battery electrodes, we replaced graphite with single-walled CNTs. Due to their unique structure, CNTs have high aspect ratio and surface area, which allows them to form efficient conductive networks with smaller weight fraction in the electrode.

We compared the performance of flexible Zn/MnO_2 batteries with MnO_2 electrode of conventional and modified compositions while keeping a commercial composition of Zn electrode. When the discharge rate was increased from C/10 to C/3, a battery with conventional electrode composition retained 60% capacity, whereas battery with modified electrode retained 93% capacity for the same discharge rates. This indicates that, despite lower fraction of conductive additive, CNTs form a more efficient conductive network that facilitates rapid kinetics of electrochemical reaction. Importantly, the modified electrode showed profound improvement in mechanical properties. It retained 97% of its capacity after being subjected to repetitive mechanical deformation. Finally, the battery with the modified electrode had high areal energy density of $4.8\,mWh\,cm^{-2}$ and volumetric energy density of $320\,mWh\,cm^{-3}$, approaching that of the commercial AA alkaline battery.

To fabricate flexible battery electrodes, we first fabricated current collector, by depositing commercially available silver ink onto the flexible polyethylene naphthalate (PEN) plastic substrate, followed by casting electrode composite on top. We used doctor blade to cast the electrodes and the current collectors, as it allows rapid deposition of inks with high solid loading. We used the AA alkaline battery electrode compositions.[30,31] Zn ink consisted of Zn as an active material, ZnO and Bi_2O_3 as corrosion inhibitors, and commercially available PSBR binder and ethylene glycol as a solvent. As Zn is highly conductive, no conductive additive is needed for Zn ink. The MnO_2 ink consisted of gamma-MnO_2 as an active material, KS6 graphite as a conductive additive, and PSBR binder and water as a solvent. The electrodes were sandwiched into a flexible battery stack, as shown in **Figure 1**a. Figure 1b shows galvanostatic discharge curves for the battery operated at C/10, C/5, and C/3 rates. We observe two discharge regions, defined by plateaus on the curves, corresponding to two MnO_2 reduction reactions. We access considerably more capacity during the first electron reaction than during the second. This is expected because the product of the second reaction – $Mn(OH)_2$ – precipitates on the surface of the graphite. $Mn(OH)_2$ is a poor electronic conductor; therefore, as the layer builds up, the resistance increases to the point where no more reduction of species can occur, thus causing electrode failure.[56–59] As the discharge rate increases, losses due to polarization increase for both reactions. Specific discharge capacity decreased from $265\,mAh\,g^{-1}$ at C/10 to ≈$210\,mAh\,g^{-1}$ at C/5 to $165\,mAh^{-1}$ at C/3 resulting in ≈38% capacity loss, which compromises utilization of this battery in high rate applications. We will further demonstrate how the rate capability can be

**ADVANCED
SCIENCE NEWS**

www.advancedsciencenews.com

Energy Technology
Generation, Conversion, Storage, Distribution

www.entechnol.de

(a)

(b)

Figure 1. a) Schematic of the flexible battery stack. b) Galvanostatic discharge curves for the battery operated at C/10, C/5, and C/3 rates. Two discharge regions defined by plateaus on the curves correspond to two MnO_2 reduction reactions. Electrode shows 60% capacity retention when discharge rate is increased from C/10 to C/3.

improved by replacing the graphite with a more efficient conductive additive – CNTs.

The thickness of the MnO_2 electrode is ≈4 times higher than that of the Zn electrode, making it more prone to failure. Therefore, the MnO_2 electrode limits the mechanical performance of the battery. When the battery is flexed, the electrode experiences tensile and compressive stresses. The possible structural failures caused by these stresses are delamination of the active layer from the current collector and formation of cracks in the layer. Delamination takes place when the shear stress at the interface exceeds a critical value; cracking occurs when tensile stress exceeds the tensile strength of the electrode composite. Electrochemical performance and mechanical performance in a battery are coupled. The delamination or cracking of the active layers leads to an Ohmic potential drop at the start of discharge. Flexing can also lead to increase in charge transfer resistance due to loss of contact between conductive additive and active material, as well as to formation of inactive phases like spinel, due to non-uniform potential distribution in the electrode.[15]

To evaluate the effect of mechanical load on the electrochemical performance of the battery, we subjected it to the series of flexing cycles before discharge. The battery was wrapped around 0.5-in. radius cylinder 100 times while keeping MnO_2 electrode in tension. **Figure 2**a shows the galvanostatic discharge curves of the battery that was discharged without flexing compared with that of the battery discharged after being flexed. As a result of flexing, capacity decreases to 23% of its original value. To elucidate the cause of failure, we conducted electrochemical impedance spectroscopy (EIS) measurements on the flat battery and battery that has undergone flexing. Figure 2b shows EIS curves for two cases. The shape of the EIS curves is consistent with the typical impedance plot for Zn/MnO_2 battery.[60] It resembles a semicircle in the high-frequency region, dominated by kinetics and a tail in a low-frequency region, dominated by mass transfer. The first interception of the semicircle corresponds to Ohmic potential drop and the second – to charge transfer polarization, and the low-frequency region – to diffusion-controlled processes. EIS data show the significant increase in charge transfer

resistance of the battery, indicated by the increase in the radius of the semicircle. This is the evidence of loss of contact between particles, which leads to loss of electrical pathways within the electrode. This indicates that the commercial binder has poor adhesion properties and is not maintaining the mechanical integrity of the electrode. The top-down scanning electron microscopy (SEM) images of the electrodes before and after flexing are shown in Figure S2, Supporting Information.

Thus, analysis of the electrochemical performance of the battery operated at different conditions showed that the battery looses 40% of its capacity when the discharge rate increased from C/10 to C/3, and 77% as a result of mechanical stress. This served as a motivation for design of the alternative electrode composition that addresses these limitations.

As previously discussed, cracking and delamination of the MnO_2 cathode limit the mechanical performance of flexible batteries based on the Zn/MnO_2 chemistry. The conventional MnO_2 electrode composite comprises gamma-MnO_2 as an active material, graphite as a conductive additive, and PSBR binder and water as a solvent. Binder that can accommodate mechanical deformation of the electrode and has strong adhesion to the electroactive particles and the conductive additive is a critical component of the composite. PSBR binder film disintegrates in the electrolyte. This results in the poor mechanical performance of the MnO_2 electrode with conventional composition.

As an alternative to PSBR, we designed the polymer gel binder that forms a 3D interpenetrated polymer network throughout the electrode, confining active material and conductive additive particles. Particularly, we used PVA/PAA polymer gel that was cross-linked in situ with the rest of the electrode components via thermal treatment. It has been shown that when exposed to temperatures ranging from 150 to 180 °C, solution of PVA and PAA undergoes condensation reaction where –COOH groups of PAA react with OH groups of PVA[47] forming interpenetrated polymer network (**Figure 3**a). A low molecular weight PAA (2000) was used to facilitate chain mobility of PAA within PVA. The mechanical properties of the resulting PVA/PAA films
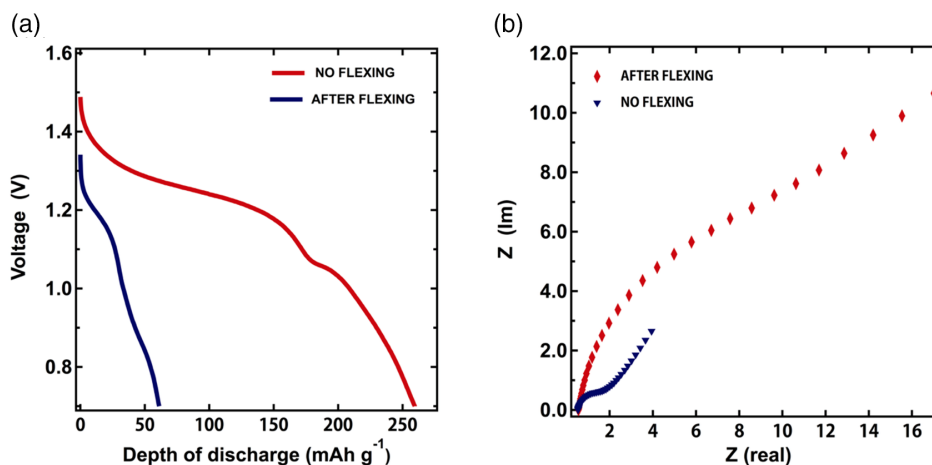
Figure 2. a) Galvanostatic discharge curves of the battery discharged without flexing compared with the battery discharged after being wrapped around 0.5-in. radius cylinder 100 times while keeping MnO_2 electrode in tension. Capacity decreases to 23% of its original value as a result of flexing. b) Data for EIS measurements on the flat battery and the battery that has undergone flexing.
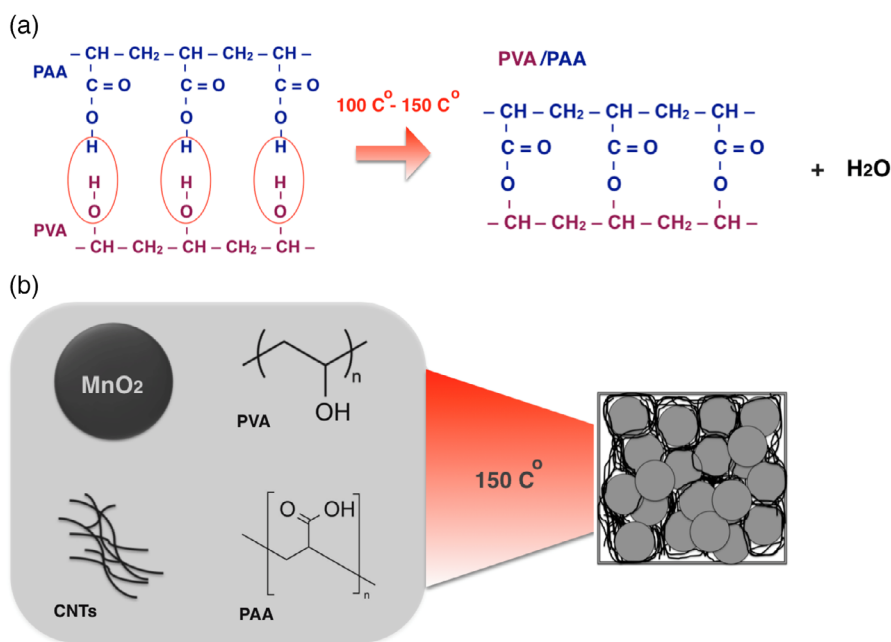
Figure 3. a) Schematics of the condensation reaction between PVA and PAA. —COOH groups of PAA react with —OH groups of PVA forming interpenetrated polymer network. b) Components and process parameters of the modified electrode: PVA is dissolved in water, CNTs are added to the mixture and ultrasonicated, followed by addition of MnO_2 and PAA. The slurry is casted onto the current collector and baked at 150 °C for 1 h.

can be controlled by varying heat treatment conditions and the ratio of the polymers. The PAA ratio of 15–20% was determined as optimum by Rhim et al.[47] by measuring the glass transition temperature (T_g) of the cross-linked PVA/PAA membranes. The T_g value increases with increasing PAA content until the PAA fraction reaches 15%, remaining nearly constant beyond 15%. This indicates that addition of PAA beyond 15% has minimal effect on the cross-linking reaction. The same authors used measurement of changes in T_g to show that the amount of time required to complete reaction at 150–180 °C is 45 min to 1 h. In addition, the content of PAA impacted mechanical properties

of the PVA/PAA membranes. The higher tensile modulus was observed for higher PAA fraction. At the same time, the tensile strength increased with increasing PAA fraction up to 15% of PAA content and then gradually decreased due to brittleness of the samples. Thus, the optimum conditions for preparing PVA/PAA membranes were achieved by treating PVA and 2000 molecular weight PAA in the ratio 85:15 at 150–180 °C for 45 min to 1 h. We used the aforementioned information to define the polymer content and processing conditions of the electrode. The modified electrode composite contained PVA/PAA in the ratio 85:15 and was baked at 150 °C for 1 h.

**ADVANCED
SCIENCE NEWS**

www.advancedsciencenews.com

Energy Technology
Generation, Conversion, Storage, Distribution

www.entechnol.de

Fourier-transform infrared spectroscopy (FTIR) data supporting the PVA/PAA cross-linking reaction is shown in Figure S1, Supporting Information.

To improve rate capability of the electrode and decrease the fraction of conductive additive, we replaced graphite with CNTs. The fiber-like structure of CNTs, their high aspect ratio, and conductivity allow establishing effective electrical percolation network at a lower weight loading than conventional carbons.[61,62] We replaced 10% mass fraction of KS6 graphite with the 1% mass fraction of CNTs. This mass fraction has been shown to be optimum for Li-ion battery systems.[61] Due to the hydrophobic nature of CNTs, they are poorly dispersible in water – the solvent used to prepare the MnO_2 electrode. However, PVA and PAA binder components can serve as surfactants that facilitate the dispersion of CNTs. Alkyl chains act as hydrophobic component and absorb on the surface of CNTs, whereas hydrophilic segments stretch into the water.[63] Polymer also increases the viscosity of the solution, and thus inhibits reaggregation of CNTs after dispersion. As PVA comprises the major part of the binder mixture (85%) and PAA serves primarily as a cross-linker, we used PVA dissolved in water as a base for CNT formulation.

Ultrasonication was used to separate nanotube clusters in the PVA/CNT suspension. Ultrasonication conditions are one of the defining parameters of the CNT/polymer formulation and final composite composition. Ultrasonication delivers shear stress to CNT's surface, through creation and imploding of bubbles in the vicinity of CNTs. Shear stress leads to separation of CNT aggregates, but at the same time can induce pulling effect on the nanotubes and can lead to fracture of the nanotubes.[64] Improvement in dispersion has been shown to have the reverse effect on the conductivity. The composite morphology with phase-separated clusters of CNTs has been shown to have more effective electron transport than homogeneous CNT network.[65] Thus, under strong shearing conditions composites mixed for less time are expected to have higher conductivity due to 1) avoiding damage of nanotubes and 2) resulting in CNT aggregates that facilitate electron transport. We limited ultrasonication time of PVA/CNT solution to 20 min, at the midrange amplitude of 40% using a Branson Digital Sonifier probe. No precipitation was observed in CNT/PVA mixture for at least 24 h after dispersion. The aforementioned considerations were taken into account when preparing the electrode slurry. To facilitate the CNT dispersion, PVA was first dissolved in water, after which CNTs were added to the mixture and ultrasonicated, followed by addition of MnO_2 and PAA. The slurry was casted onto the current collector and baked at 150 °C for 1 h (Figure 3b). The resulting electrode was combined with the rest of the battery components to form the flexible battery.

Figure 4a shows image of the 90 μm thick MnO_2 electrode casted on flexible current collector. The electrode can be readily flexed without cracking or delamination. The galvanostatic discharge curves of the battery with MnO_2 electrode composite comprising PVA/PAA binder and CNT conductive additive are shown in Figure 4b. The data for the battery with standard electrode composition discharged under the same conditions are shown in Figure 1b. At C/10, both batteries show similar specific capacity of 270 and 265 mAh g^{-1}, respectively. However, the specific discharge capacity of the battery with the standard

electron composition decreases from 265 mAh g^{-1} at C/10 to ≈210 mAh g^{-1} at C/5 to 165 mAh g^{-1} at C/3 resulting in ≈40% capacity loss. At the same time, the battery with the modified MnO_2 electrode retains 93% of capacity when the discharge rate is increased from C/10 to C/3, with slight decrease in capacity from 270 mAh g^{-1} at C/10 to ≈260 mAh g^{-1} at C/5 to 250 mAh g^{-1} at C/3. Thus, MnO_2 electrode fabricated using modified approach shows 93% capacity retention when discharge rate is increased from C/10 to C/3, compared with ≈60% capacity retention in the battery with the conventional electrode composition. This indicates that CNTs form more efficient conductive network than graphite facilitating high kinetics of electrochemical reaction. Replacing KS6 graphite with CNTs also allows reducing the weight fraction of conductive additive in the electrode from 10% to 1%.
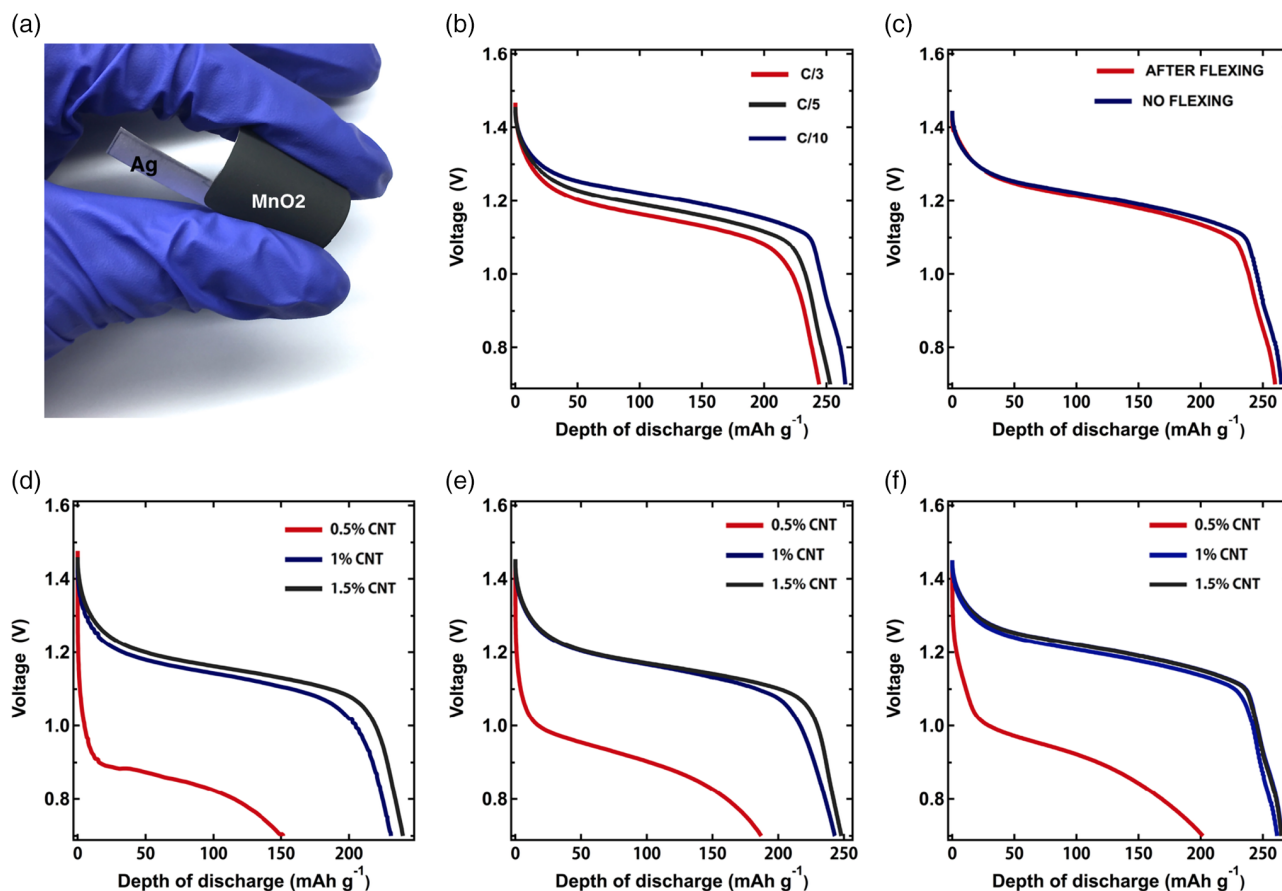
Analyzing the shape of the discharge curves for both batteries we observe that the discharge curves of the battery with the modified electrode composition have flatter plateau with lower potential. Lower plateau potential confirms the formation of the MnOOH oxide on the surface of MnO_2 particles during thermal treatment.[66,67] At C/10, 20% more capacity is accessed during the first electron reaction in the modified case, in comparison to the conventional case. The second electron reaction is almost absent in the modified case, while it constitutes ≈20% of the overall capacity in the conventional case.

The reason can be elucidated by revisiting the mechanism for the second MnO_2 reduction step. Reduction proceeds via dissolution–precipitation mechanism.[57,66] Mn^{3+} species dissolve in the electrolyte and get reduced to Mn^{2+} when they come in contact with the conductive surface. As the solubility of Mn^{2+} is much lower than that of Mn^{3+}, any Mn^{2+} species generated will precipitate as $Mn(OH)_2$ on the surface of the electronic conductor forming a layer that eventually occludes the ion transport to the conductor and, thus, terminates the reaction. If PVA/PAA binder coats MnO_2 particles, then Mn^{3+} and Mn^{2+} ions are trapped in the vicinity of the particles and reach the solubility limit significantly faster. Thus, we can expect Mn^{2+} to precipitate almost immediately on the surface on CNTs in the vicinity of the particles, hindering further reaction.

The modified electrode shows significant improvement in mechanical properties. Figure 4c compares galvanostatic discharge curve of the flat battery with the curve of the battery that was subjected to the series of flexing cycles before discharge. The battery shows capacity retention of 97% after being wrapped around 0.5-in. radius cylinder 100 times while keeping the MnO_2 electrode in tension. In contrast, the battery with standard electrode composition (Figure 2a) loses 77% of its capacity after being flexed at the same conditions.

To further optimize the fraction of the conductive additive in the MnO_2 electrode, we varied the CNT fraction in the composite. The effect of CNT weight fraction on the performance of the battery discharged at C/3, C/5, and C/10 rates is shown in Figure 4d–f, respectively. For all rates, discharge capacity of the battery decreases when the CNT weight fraction is decreased from 1% to 0.5% (175, 200, and 225 mAh g^{-1} discharge capacity for the battery with 0.5% CNT content for C/3, C/5, and C/10, respectively; 240, 253, and 270 mAh g^{-1} discharge capacity for the battery with 1% CNT for the same rates). When the CNT fraction is increased from 1% to 1.5%, the discharge capacity

**ADVANCED
SCIENCE NEWS**

www.advancedsciencenews.com

Energy Technology
Generation, Conversion, Storage, Distribution

www.entechnol.de

Figure 4. a) Image of the 90 µm thick MnO_2 electrode printed on the flexible current collector. b) Galvanostatic discharge curves for the battery operated at C/10, C/5, and C/3 rates. MnO_2 electrode fabricated using modified approach shows 93% capacity retention when discharge rate is increased from C/10 to C/3. c) Galvanostatic discharge curves of the battery discharged without flexing compared with the battery discharged after being flexed. The battery shows capacity retention of 97% after being wrapped around 0.5-in. radius cylinder 100 times while keeping MnO_2 electrode in tension. Galvanostatic discharge curves for the batteries with 0.5%, 1%, and 1.5% CNTs operated at d) C/3, e) C/5, and f) C/10 rates.

increases from 240 to 250 mAh g^{-1} for C/3 discharge rate, and remains nearly unchanged at ≈253 and ≈270 mAh g^{-1} at C/5 and C/10 rates, respectively. As seen from the voltage values of the discharge curves, lowering CNT concentration from 1 to 0.5 wt% results in the potential drop of 0.3, 0.22, and 0.18 V for C/3, C/5, and C/10, respectively. Consequently, energy efficiency of the batteries with lower CNT content is reduced. Decrease in the electrode conductivity as the CNT content is reduced causes this drop. Therefore, a weight fraction of 0.5% is not sufficient to create an effective conductive network in the MnO_2 electrode composite and the higher fraction of CNT is desirable for optimum battery performance. On the contrary, increasing CNT weight fraction from 1% to 1.5% does not result in energy efficiency increase for slower operating rates of C/5 and C/10; 4% capacity gain is observed at C/3. Thus, if the battery is expected to operate at low rates, increasing CNT fraction beyond 1% does not add value in terms of energy efficiency.

Figure 5 shows SEM images of the cross-sectional (a,d) and top (b,c,e,f,) view of the electrodes with conventional (a–c) and modified (d–f) compositions. The image of the conventional electrode shows that graphite particles are homogeneously dispersed throughout the composite. However, the particles are

neither connected between themselves, nor do they seem to adhere to MnO particles. The images of the modified electrode show that PVA/PAA/CNT composite homogeneously coats MnO_2 particles. CNTs are incorporated into the polymer. In addition, we can clearly see the polymer bridges between the particles – holding the structure together. Thus, analysis of the SEM images supports the hypothesis regarding the mechanical failure mechanism of the electrode with conventional electrode composition: due to loss of contact between particles, which leads to loss of electrical pathways within the electrode. It also confirms that PVA/PAA/CNT forms 3D interpenetrated polymer network throughout the electrode, confining the active material.

This work elaborates on design of the electrode composite for flexible Zn/MnO_2 batteries, with the goal of improving mechanical and electrochemical performance, as well as specific energy density of the battery. To improve flexibility, we chose PVA in situ cross-linked with PAA as a polymer binder for the MnO_2 electrode. PAA/PVA composite is chemically compatible with KOH electrolyte used in Zn/MnO_2 chemistry and permeable to it. It also exhibits high tensile strength without brittleness, which are desired mechanical properties for the binder. To improve rate capability of the electrode and decrease the fraction
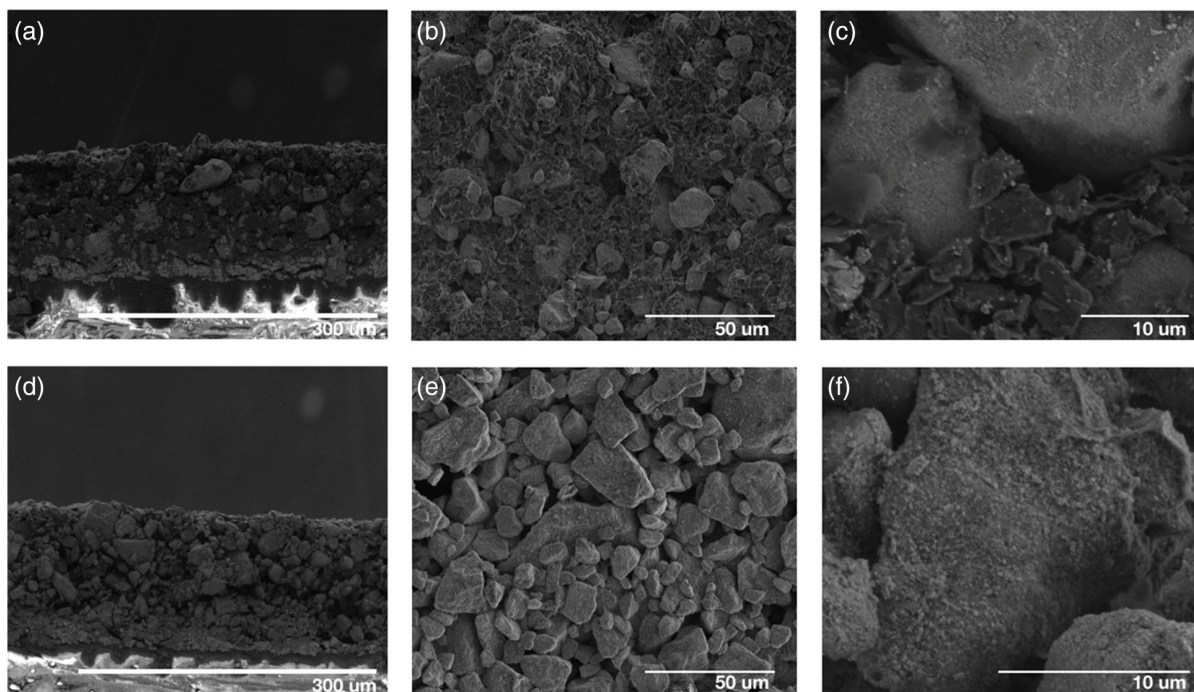
Figure 5. SEM images of the cross-sectional a,d) and top b,c,e,f) views of the electrodes with conventional a–c) and modified d–f) compositions.

of conductive additive, we replaced graphite with CNTs. Resulting electrode comprised polymer network with enclosed MnO_2 particles and conductive network of CNTs. Battery fabricated with MnO_2 electrode based on CNT/PVA/PAA composite showed improved capacity retention when discharged at high rates, and profound improvement in mechanical properties compared with the batteries with conventional electrode composition. It retained 93% capacity when the discharge rate was increased from C/10 to C/3, as well as 97% of its capacity after being flexed. In contrast, batteries based on conventional composition retained 60% and 23%, respectively. The battery with the modified electrode had a high areal energy density of $4.8\,mWh\,cm^{-2}$. The volumetric energy density of $320\,mWh\,cm^{-3}$ approached that of the commercial device ($350\,mWh\,cm^{-3}$).

Similar battery electrode fabrication approach could be explored to achieve flexible MnO_2 electrodes in rechargeable Zn/MnO_2 battery systems, which have been receiving a great deal of attention.[16,68] MnO_2 electrodes in these systems are subject to volume change due to Zn intercalation.[16] This causes structural disintegration of the electrodes during cycling. Fabricating electrodes through in situ cross-linking of PVA and PAA results in formation of the polymer coating on the surface of the particles. This coating might potentially prevent structural collapse of the particles during cycling.

In addition, based on the application requirements, increasing the battery energy density could be explored further through increasing the thickness of the electrodes. To maximize the mechanical flexibility of the thicker electrodes, their composition has to be fine-tuned to achieve optimum cohesion strength of the electrode and its adhesion to the current collector. Overall, protocols to measure the adhesion and cohesion strength of composite battery electrodes are not standardized. As a result, researches

adopted and modified various mechanical testing methods.[69–72] For example, Gaikwad et al. used the modified peel test and drag test as tools to investigate the effect of the electrode formulation on the mechanical strength of the electrodes.[71] These testing methods could be used to further study the effect of changing the electrode composition on the mechanical strength of the electrodes fabricated through in situ polymerization of PVA/PAA.

Experimental Section

To prepare a current collector, a doctor blade was used to deposit a 10 μm Ag ink layer (Creative Materials 118-09) on the PEN substrate (DuPont). The substrate was then baked at 125 °C for 30 min. The thickness of the Ag layer after the baking step was approximately 5 μm. The MnO_2 ink of conventional composition was prepared as previously described elsewhere.[31] Briefly, ink consisted of a mixture (by dry weight) of 80% MnO_2 (Tronox), 10% graphite (KS6, Timcal), and 10% polystyrene binder (LICO Technology Corp.). Deionized water (DI) water was used as a solvent. The Zn ink was a mixture (by weight) of 69.3% Zn (Sigma-Aldrich), 7.3% ZnO nanopowder (Inframat), 10.9% Bi_2O_3 (Alfa Aesar), 10.9% ethylene glycol, and 1.6% polystyrene binder. The inks were casted on the silver current collector and baked in an oven at 100 °C for 60 min to remove the solvent. The MnO_2 ink of modified composition was prepared as follows: 0.1 g of PVA (31 000–50 000 MW; Sigma-Aldrich) was dissolved in 2.4 g DI water; after that 0.04 g of CNTs from Carbon Solutions, Inc. in the form of iP-single-walled CNTs was added to the mixture and ultrasonicated for 20 min at the amplitude 40%. 3.98 g of MnO_2 and 0.019 g of PAA were added to the mixture and mixed using Vortex mixer for 5 min at 3000 rpm. The slurry was casted onto the current collector and baked at 150 °C for 60 min. MnO_2 electrodes were 1 in.^{2} in area, 90–100 μm thick, with MnO_2 loading of ≈0.1 g electrode^{-1}. Zn electrodes were 1 in.^{2} in area, ≈20 μm thick, with Zn loading of ≈0.04 g electrode^{-1}. The battery was MnO_2 limited with the total cell capacity of ≈27 mAh (Figure S3, Supporting Information).

A solution of KOH (5.6 M) and ZnO (0.37 M) was used as the electrolyte, which was prepared by mixing KOH pellets and ZnO powder in DI water. The mixture was stirred until a clear solution formed. A PVA/cellulose wet-laid nonwoven material soaked in the electrolyte was used as a separator (Freudenberg Vliesstoffe KG, Germany). The electrodes and the separator were cut to a size of 1 in.² with extended tabs to connect to the battery. The separator was sandwiched between the two electrodes and the cell was heat sealed between two layers of PVC (75 mm; McMaster). The contact between the tab and the PVC sheet was sealed with double-sided tape (3 M). The tape was stable in high-pH solutions. The assembled battery was discharged using a battery tester (MTI Corp.). The EIS measurements were performed using a Gamry potentiostat. SEM was performed using a TM3000 (Hitachi).

Supporting Information

Supporting Information is available from the Wiley Online Library or from the author.

Conflict of Interest

The authors declare no conflict of interest.

[1] Y. Khan, A. E. Ostfeld, C. M. Lochner, A. Pierre, A. C. Arias, *Adv. Mater.* **2016**, *28*, 4373.
[2] S. L. Swisher, M. C. Lin, A. Liao, E. J. Leeflang, Y. Khan, F. J. Pavinatto, K. Mann, A. Naujokas, D. Young, S. Roy, M. R. Harrison, A. C. Arias, V. Subramanian, M. M. Maharbiz, *Nat. Commun.* **2015**, *6*, 6575.
[3] T. R. Ray, J. Choi, A. J. Bandodkar, S. Krishnan, P. Gutruf, L. Tian, R. Ghaffari, J. A. Rogers, *Chem. Rev.* **2019**, *119*, 5461.
[4] J. S. Heo, J. Eom, Y.-H. Kim, S. K. Park, *Small* **2018**, *14*, 1703034.
[5] Y. Liu, M. Pharr, G. A. Salvatore, *ACS Nano* **2017**, *11*, 9614.
[6] J. R. Corea, A. M. Flynn, B. Lechêne, G. Scott, G. D. Reed, P. J. Shin, M. Lustig, A. C. Arias, *Nat. Commun.* **2016**, *7*, 10839.
[7] C. M. Lochner, Y. Khan, A. Pierre, A. C. Arias, *Nat. Commun.* **2014**, *5*, 5745.
[8] M. E. Payne, A. Zamarayeva, V. I. Pister, N. A. D. Yamamoto, A. C. Arias, *Sci. Rep.* **2019**, *9*, 13720.
[9] S. Emaminejad, W. Gao, E. Wu, Z. A. Davies, H. Y. Y. Nyein, S. Challa, S. P. Ryan, H. M. Fahad, K. Chen, Z. Shahpar, S. Talebi, C. Milla, A. Javey, R. W. Davis, *Proc. Natl. Acad. Sci. USA* **2017**, *114*, 4625.
[10] J. Heikenfeld, *Electroanalysis* **2016**, *28*, 1242.
[11] M. Bariya, H. Y. Y. Nyein, A. Javey, *Nat. Electron.* **2018**, *1*, 160.
[12] A. M. Zamarayeva, A. E. Ostfeld, M. Wang, J. K. Duey, I. Deckman, B. P. Lechêne, G. Davies, D. A. Steingart, A. C. Arias, *Sci. Adv.* **2017**, *3*, e1602051.
[13] A. E. Ostfeld, A. C. Arias, *Flex. Print. Electron.* **2017**, *2*, 013001.
[14] A. E. Ostfeld, A. M. Gaikwad, Y. Khan, A. C. Arias, *Sci. Rep.* **2016**, *6*, 26122.
[15] A. M. Gaikwad, A. C. Arias, D. A. Steingart, *Energy Technol.* **2014**, *3*, 305.
[16] H. Li, L. Ma, C. Han, Z. Wang, Z. Liu, Z. Tang, C. Zhi, *Nano Energy* **2019**, *62*, 550.
[17] P. Tan, B. Chen, H. Xu, H. Zhang, W. Cai, M. Ni, M. Liu, Z. Shao, *Energy Environ. Sci.* **2017**, *10*, 2056.
[18] C. Guan, A. Sumboja, H. Wu, W. Ren, X. Liu, H. Zhang, Z. Liu, C. Cheng, S. J. Pennycook, J. Wang, *Adv. Mater.* **2017**, *29*, 1704117.
[19] J. Fu, F. M. Hassan, J. Li, D. U. Lee, A. R. Ghannoum, G. Lui, M. A. Hoque, Z. Chen, *Adv. Mater.* **2016**, *28*, 6421.
[20] Z. Pei, Y. Huang, Z. Tang, L. Ma, Z. Liu, Q. Xue, Z. Wang, H. Li, Y. Chen, C. Zhi, *Energy Storage Mater.* **2019**, *20*, 234.
[21] K. Kordek, L. Jiang, K. Fan, Z. Zhu, L. Xu, M. Al-Mamun, Y. Dou, S. Chen, P. Liu, H. Yin, P. Rutkowski, H. Zhao, *Adv. Energy Mater.* **2019**, *9*, 1802936.
[22] Q. Liu, Y. Wang, L. Dai, J. Yao, *Adv. Mater.* **2016**, *28*, 3000.
[23] F. Meng, H. Zhong, D. Bao, J. Yan, X. Zhang, *J. Am. Chem. Soc.* **2016**, *138*, 10226.
[24] M. Yu, Z. Wang, C. Hou, Z. Wang, C. Liang, C. Zhao, Y. Tong, X. Lu, S. Yang, *Adv. Mater.* **2017**, *29*, 1602868.
[25] H.-F. Wang, C. Tang, B. Wang, B.-Q. Li, X. Cui, Q. Zhang, *Energy Storage Mater.* **2018**, *15*, 124.
[26] T. Zhou, W. Xu, N. Zhang, Z. Du, C. Zhong, W. Yan, H. Ju, W. Chu, H. Jiang, C. Wu, Y. Xie, *Adv. Mater.* **2019**, *31*, 1807468.
[27] C.-Y. Su, H. Cheng, W. Li, Z.-Q. Liu, N. Li, Z. Hou, F.-Q. Bai, H.-X. Zhang, T.-Y. Ma, *Adv. Energy Mater.* **2017**, *7*, 1602420.
[28] C. Guan, A. Sumboja, W. Zang, Y. Qian, H. Zhang, X. Liu, Z. Liu, D. Zhao, S. J. Pennycook, J. Wang, *Energy Storage Mater.* **2019**, *16*, 243.
[29] Y. Jiang, Y. Deng, R. Liang, J. Fu, D. Luo, G. Liu, J. Li, Z. Zhang, Y. Hu, Z. Chen, *Adv. Energy Mater.* **2019**, *9*, 1900911.
[30] A. M. Gaikwad, H. N. Chu, R. Qeraj, A. M. Zamarayeva, D. A. Steingart, *Energy Technol.* **2013**, *1*, 177.
[31] A. M. Gaikwad, G. L. Whiting, D. A. Steingart, A. C. Arias, *Adv. Mater.* **2011**, *23*, 3251.
[32] A. M. Gaikwad, A. M. Zamarayeva, J. Rousseau, H. Chu, I. Derin, D. A. Steingart, *Adv. Mater.* **2012**, *24*, 5071.
[33] A. M. Gaikwad, D. A. Steingart, T. Nga Ng, D. E. Schwartz, G. L. Whiting, *Appl. Phys. Lett.* **2013**, *102*, 233302.
[34] W. Qiu, Y. Li, A. You, Z. Zhang, G. Li, X. Lu, Y. Tong, *J. Mater. Chem. A* **2017**, *5*, 14838.
[35] Y. Zeng, X. Zhang, Y. Meng, M. Yu, J. Yi, Y. Wu, X. Lu, Y. Tong, *Adv. Mater.* **2017**, *29*, 1700274.
[36] H.-W. Zhu, J. Ge, Y.-C. Peng, H.-Y. Zhao, L.-A. Shi, S.-H. Yu, *Nano Res.* **2018**, *11*, 1554.
[37] M. Kaltenbrunner, M. Kettlgruber, C. Siket, R. Schwödiauer, S. Bauer, *Adv. Mater.* **2010**, *22*, 2065.
[38] G. Kettlgruber, M. Kaltenbrunner, C. M. Siket, R. Moser, I. M. Graz, R. Schwödiauer, S. Bauer, *J. Mater. Chem. A* **2013**, *1*, 5505.
[39] Z. Wang, Z. Wu, N. Bramnik, S. Mitra, *Adv. Mater.* **2014**, *26*, 970.
[40] F. Mo, G. Liang, Q. Meng, Z. Liu, H. Li, J. Fan, C. Zhi, *Energy Environ. Sci.* **2019**, *12*, 706.
[41] D. Wang, L. Wang, G. Liang, H. Li, Z. Liu, Z. Tang, J. Liang, C. Zhi, *ACS Nano* **2019**, *13*, 10643.
[42] Z. Liu, D. Wang, Z. Tang, G. Liang, Q. Yang, H. Li, L. Ma, F. Mo, C. Zhi, *Energy Storage Mater.* **2019**, *23*, 636.
[43] D. Linden, *Handbook of Batteries*, McGraw-Hill, New York **2004**.

**ADVANCED
SCIENCE NEWS**

www.advancedsciencenews.com

Energy Technology
Generation, Conversion, Storage, Distribution

www.entechnol.de

[44] G. M. Wu, S. J. Lin, C. C. Yang, *J. Membr. Sci.* **2006**, *275*, 127.

[45] G. M. Wu, S. J. Lin, C. C. Yang, *J. Membr. Sci.* **2006**, *280*, 802.

[46] Z. Wang, X. Meng, Z. Wu, S. Mitra, *J. Energy Chem.* **2017**, *26*, 129.

[47] J.-W. Rhim, M.-Y. Sohn, H.-J. Joo, K.-H. Lee, *J. Appl. Polym. Sci.* **1993**, *50*, 679.

[48] A. Kovalcik, *Polymer Gels: Synthesis and Characterization*, Springer, Singapore **2018**, pp. 1–27.

[49] N. Chen, J. Zhang, *Chin. J. Polym. Sci.* **2010**, *28*, 903.

[50] K.-F. Arndt, A. Richter, S. Ludwig, J. Zimmermann, J. Kressler, D. Kuckling, H.-J. Adler, *Acta Polym.* **1999**, *50*, 383.

[51] K. Kumeta, I. Nagashima, S. S. Matsui, K. K. Mizoguchi, *J. Appl. Polym. Sci.* **2003**, *90*, 2420.

[52] E. Ruckenstein, L. Liang, *J. Appl. Polym. Sci.* **1996**, *62*, 973.

[53] H. Byun, B. Hong, S. Y. Nam, S. Y. Jung, J. W. Rhim, S. B. Lee, G. Y. Moon, *Macromol. Res.* **2008**, *16*, 189.

[54] J. Jose, F. Shehzad, M. A. Al-Harthi, *Polym. Bull.* **2014**, *71*, 2787.

[55] J. Song, M. Zhou, R. Yi, T. Xu, M. L. Gordin, D. Tang, Z. Yu, M. Regula, D. Wang, *Adv. Funct. Mater.* **2014**, *24*, 5904.

[56] S. W. Donne, G. A. Lawrance, D. A. J. Swinkels, *J. Electrochem. Soc.* **1997**, *144*, 2949.

[57] A. Kozawa, J. F. Yeager, *J. Electrochem. Soc.* **1968**, *115*, 1003.

[58] J. W. Gallaway, B. J. Hertzberg, Z. Zhong, M. Croft, D. E. Turney, G. G. Yadav, D. A. Steingart, C. K. Erdonmez, S. Banerjee, *J. Power Sources* **2016**, *321*, 135.

[59] B. J. Hertzberg, A. Huang, A. Hsieh, M. Chamoun, G. Davies, J. K. Seo, Z. Zhong, M. Croft, C. Erdonmez, Y. S. Meng, D. Steingart, *Chem. Mater.* **2016**, *28*, 4536.

[60] S. W. Donne, J. H. Kennedy, *J. Appl. Electrochem.* **2004**, *34*, 159.

[61] B. J. Landi, M. J. Ganter, C. D. Cress, R. A. DiLeo, R. P. Raffaelle, *Energy Environ. Sci.* **2009**, *2*, 638.

[62] B. J. Landi, R. P. Raffaelle, M. J. Heben, J. L. Alleman, W. VanDerveer, T. Gennett, *Nano Lett.* **2002**, *2*, 1329.

[63] J. Ning, J. Zhang, Y. Pan, J. Guo, *Ceram. Int.* **2004**, *30*, 63.

[64] Y. Y. Huang, T. P. J. Knowles, E. M. Terentjev, *Adv. Mater.* **2009**, *21*, 38.

[65] Y. Y. Huang, E. M. Terentjev, Y. Y. Huang, E. M. Terentjev, *Polymers* **2012**, *4*, 275.

[66] D. Boden, C. J. Venuto, D. Wisler, R. B. Wylie, *J. Electrochem. Soc.* **1967**, *114*, 415.

[67] A. Kozawa, *J. Electrochem. Soc.* **1959**, *106*, 79.

[68] P. Yu, Y. Zeng, H. Zhang, M. Yu, Y. Tong, X. Lu, *Small* **2019**, *15*, 1804760.

[69] B. Son, M.-H. Ryou, J. Choi, T. Lee, H. K. Yu, J. H. Kim, Y. M. Lee, *ACS Appl. Mater. Interfaces* **2014**, *6*, 526.

[70] A. J. Blake, R. R. Kohlmeyer, L. F. Drummy, J. S. Gutiérrez-Kolar, J. Carpena-Núñez, B. Maruyama, R. Shahbazian-Yassar, H. Huang, M. F. Durstock, *ACS Appl. Mater. Interfaces* **2016**, *8*, 5196.

[71] A. M. Gaikwad, A. C. Arias, *ACS Appl. Mater. Interfaces* **2017**, *9*, 6390.

[72] H. Li, Z. Tang, Z. Liu, C. Zhi, *Joule* **2019**, *3*, 613.

1901165 (9 of 9)